JMEPEG (2018) 27:728–738
https://doi.org/10.1007/s11665-018-3168-2

1059-9495/$19.00

Constitutive Model for Hot Deformation of the Cu-Zr-Ce Alloy

Yi Zhang, Huili Sun, Alex A. Volinsky, Bingjie Wang, Baohong Tian, Yong Liu, and Kexing Song

(Submitted August 21, 2017; in revised form September 5, 2017; published online January 19, 2018)

Hot compressive deformation behavior of the Cu-Zr-Ce alloy has been investigated according to the hot deformation tests in the 550-900 °C temperature range and 0.001-10 s^{-1} strain rate range. Based on the true stress–true strain curves, the flow stress behavior of the Cu-Zr-Ce alloy was investigated. Microstructure evolution was observed by optical microscopy. Based on the experimental results, a constitutive equation, which reflects the relationships between the stress, strain, strain rate and temperature, has been established. Material constants n, α, Q and ln A were calculated as functions of strain. The equation predicting the flow stress combined with these materials constants has been proposed. The predicted stress is consistent with experimental stress, indicating that developed constitutive equation can adequately predict the flow stress of the Cu-Zr-Ce alloy. Dynamic recrystallization critical strain was determined using the work hardening rate method. According to the dynamic material model, the processing maps for the Cu-Zr and Cu-Zr-Ce alloy were obtained at 0.4 and 0.5 strain. Based on the processing maps and microstructure observations, the optimal processing parameters for the two alloys were determined, and it was found that the addition of Ce can promote the hot workability of the Cu-Zr alloy.

Keywords annealing, Cu-Zr-Ce alloy, processing map, transmission electron microscopy (TEM)

1. Introduction

Copper alloys have superior electrical and thermal conductivity, good corrosion resistance and high strength. They are widely used in many applications (Ref 1), such as railway contact wires (Ref 2), diverter target materials (Ref 3) and electronic components (Ref 4). Many research results have been shown where aging strengthening of copper alloys can be achieved, based on optimized required performance (Ref 5, 6). Several precipitation-strengthened copper alloys, which have good strength and conductivity, have been reported, including Cu-Fe-P (Ref 7), Cu-Cr-Zr (Ref 6) and Cu-Ni-Si (Ref 8) alloys.

Due to the addition of small Zr amounts, Cu-Zr alloy has good strength and conductivity (Ref 3, 9). Some recent reports (Ref 10, 11) have studied aging characteristics of the Cu-Zr alloy. For the Cu-0.5%Zr-0.065%B alloy, Ye et al. (Ref 10) found that the tensile strength can reach 575.4 MPa after two steps of deformation aging process, and conductivity can achieve 79.37% IACS (International Annealed Copper Standard). According to the research results, Ye et al. also reported that the high strength and conductivity were attributed to the Cu_5Zr aging precipitate phase with face-centered cubic structure. Peng et al. (Ref 9) also found that the precipitation in the Cu-0.12Zr alloy aged at 450 °C is coherent face-centered cubic Cu_5Zr phase, determined by indexing the selected area electron diffraction pattern. Phillips (Ref 12) studied the Cu-1.07%Zr alloy, which was treated with plastic deformation and aging treatment at 850 °C, and concluded that the Cu_5Zr was the precipitating phase, which was the reason for the high hardness. The strengthening mechanism of the Cu-Cr-Zr alloy aged at 450 °C for 4 h was investigated by Wang et al. (Ref 13), and the results showed that the precipitates (Cu_4Zr and Cu_5Zr) can increase the hardness.

Many researchers showed that the hot rolling treatment affects the final product quality through microstructure evolution (Ref 14). However, little research on studying hot compressive behavior of Cu-Zr alloy was found (Ref 13). Thus, obtaining the relationships between the thermo-mechanical processing parameters, such as strain rate, deformation temperature and strain, and their effects on hot compressive characteristics is beneficial for production of the Cu-Zr alloy. Various constitutive equations, predicting the relationships between the hot working parameters, have been proposed to describe the relationships between temperature, strain and strain rate. These constitutive equations included physically based models, artificial neural network and phenomenological models (Ref 15-17). Famous phenomenological model was put forward by McTegart and Sellars (Ref 18), which is the relationship between the strain rate, flow stress and temperature described by the Arrhenius type equation, an approach which was expressed by the hyperbolic sine function. In recent years, some researchers found that the strain has an effect on the coefficients of the Arrhenius equation, and tried to modify this equation (Ref 19, 20).

In this paper, the aim is to study the flow behavior of the Cu-0.2Zr-0.15Ce alloy under various hot compression conditions. According to the experimental data, a constitutive equation reflecting the effects of the strain rate, temperature and strain has been developed to reflect the flow stress of the alloy. The dynamic recrystallization (DRX) critical strain for this alloy

Yi Zhang, Huili Sun, Bingjie Wang, Baohong Tian, Yong Liu, and **Kexing Song,** School of Materials Science and Engineering, Henan University of Science and Technology, Luoyang 471003, China; and Collaborative Innovation Center of Nonferrous Metals, Luoyang 471003 Henan Province, China; and **Alex A. Volinsky,** Department of Mechanical Engineering, University of South Florida, Tampa, FL 33620, USA. Contact e-mails: zhshgu436@163.com; shllt0909@126.com

was determined. Processing maps at 0.4 and 0.5 strain, based on the dynamic material model (DMM) for the Cu-0.2%Zr-0.15%Ce and Cu-0.2%Zr alloys were developed to determine the optimal hot working process parameters.

2. Experimental Details

The Cu-0.2%Zr and Cu-0.2%Zr-0.15%Ce alloys were obtained by melting in a vacuum induction furnace in argon. The chemical components were 0.2Zr, 0.15Ce and Cu balance in wt.%. In order to avoid the alloying microsegregation, the ingot was treated at 920 °C for 2 h. To preserve the supersaturated solid solution structure of the Cu-0.2%Zr(-0.15%Ce) alloy, solution heat treatment was performed at 900 °C for 1 h, and then it was water-quenched. Specimens with Φ12 mm × 8 mm dimensions were machined from the ingot with the cylinder axis parallel to the rolling direction for the hot compression tests.

With the Gleeble-1500D thermo-mechanical simulator, the thermal deformation simulation tests were performed. The test temperature was 550-900 °C, and the strain rate was 0.001-10 s^{-1}. The specimens were heated up to 1000 °C, with a heating rate of 20 °C/s and kept for 6 min to obtain uniformly distributed temperature throughout the sample before compression. Then, the temperature reached the set value. In order to minimize the friction effects, graphite tantalum sheets were placed at the ends of the cylindrical sample. All specimens were compressed to a total true strain of 0.7. After deformation, the high-temperature deformation microstructure was immediately preserved by water quenching. Then, the microscopic test samples were prepared by sectioning the compressed specimens along the compression axis. All compressed specimens were polished and then etched with corrosive liquid of 5 g $FeCl_3$ + 85 mL alcohol + 10 mL HCl. The microstructure was observed with the Olympus PMG3 optical microscope. Gatan 691 ion beam thinner was used to prepare the TEM samples. The JEM-2100 high-resolution transmission electron microscope (HRTEM) was utilized to observe the transmission electron micrographs (TEM).

3. Results and Discussion

3.1 Flow Stress Behavior Analysis

The true stress–true strain curves of the Cu-0.2%Zr-0.15%Ce alloy at different compressive deformation conditions are shown in Fig. 1. The flow stress can be strongly affected by the test temperature and the strain rate during hot deformation. It can be seen from Fig. 1 that the flow stress value is escalating with the strain rate increase and moving down with the deformation temperature increase. During hot deformation, the hot compressive deformation mechanisms can be classified as work hardening, dynamic recovery (DRV) and dynamic recrystallization (DRX). The hot deformation test temperature and strain rate have a great influence on the microstructure and performance of the studied alloy.

According to Fig. 1, the true flow stress increases sharply at the initial deformation stage, which indicates that the effect of work hardening on the flow stress is stronger than dynamic softening. With continued deformation, the key compressive mechanism for hot compression is dynamic recovery at lower temperatures. At 550 °C and 0.01 s^{-1}, smooth flow stress curves can be observed with the increasing strain. These stable curves represent the balance between the dynamic softening and work hardening, which is the characteristic of the dynamic recovery. Zhang et al. (Ref 21) have observed the same DRV phenomenon at lower temperatures by studying the Cu-Cr-Zr-Y alloy. Another kind of phenomenon is dynamic recrystallization, which was observed at high temperature, because higher temperature can improve the atomic kinetic energy and atomic vibration amplitude (Ref 22). For example, at 900 °C, the flow stress reaches a maximum value and then reduces to a relatively stable value. However, at the same temperature, compared with the high strain rate of 10 s^{-1}, the stress value is smaller for the low strain rate of 0.1 s^{-1}. The reason is because there is enough time for softening and dislocations annihilation to eliminate the stress at low strain rate.

3.2 Constitutive Modeling Analysis

Arrhenius equation is widely used to interpret the connections between the flow stress, deformation temperature and strain rate. For the hot compression test, the relationship between the flow stress (σ), strain rate ($\dot{\varepsilon}$) and temperature (T) can be expressed as (Ref 23):

$$\dot{\varepsilon} = A_1 \sigma^{n_1} \exp\left(-\frac{Q}{RT}\right), \quad \text{(Eq 1)}$$

$$\dot{\varepsilon} = A_2 \exp(\beta\sigma) \exp\left(-\frac{Q}{RT}\right), \quad \text{(Eq 2)}$$

$$\dot{\varepsilon} = A[\sinh(\alpha\sigma)]^n \exp\left(-\frac{Q}{RT}\right), \quad \text{(Eq 3)}$$

$$Z = \dot{\varepsilon} \exp\left(\frac{Q}{RT}\right). \quad \text{(Eq 4)}$$

Here, $\dot{\varepsilon}$ is the strain rate (s^{-1}), σ—flow stress (MPa), R—universal gas constant (8.314 J mol^{-1} K^{-1}), Q—activation energy for hot deformation (kJ mol^{-1}), T—absolute temperature (K), A (s^{-1}), A_1, A_2, n_1, n and α (MPa^{-1})—materials constants, and $\alpha = \beta/n_1$, which can be calculated by linear regression analysis.

By calculating natural logarithms of the two sides of Eq 1 and 2, the following equations can be obtained:

$$\ln\sigma = \frac{\ln\dot{\varepsilon}}{n_1} - \frac{\ln A_1}{n_1} - \frac{Q}{n_1 RT}, \quad \text{(Eq 5)}$$

$$\sigma = \frac{\ln\dot{\varepsilon}}{\beta} - \frac{\ln A_2}{\beta} + \frac{Q}{\beta RT}. \quad \text{(Eq 6)}$$

According to Eq 5 and 6, a linear relationship exists between $\ln\dot{\varepsilon}$ and $\ln\sigma$, and even between $\ln\dot{\varepsilon}$ and σ. The relationships of $\ln\dot{\varepsilon}$-$\ln\sigma$ (with the linear slope n_1) and $\ln\dot{\varepsilon}$-σ (with the linear slope β) under test temperatures are shown in Fig. 2(a) and (b). It can be seen that some straight lines are almost parallel to each other in Fig. 2. By calculating the average values of the slopes, the values of n_1 and β are 19.493 and 0.278 MPa^{-1}, respectively. Thus, $\alpha = \beta/n_1 = 0.0143$ MPa^{-1}.

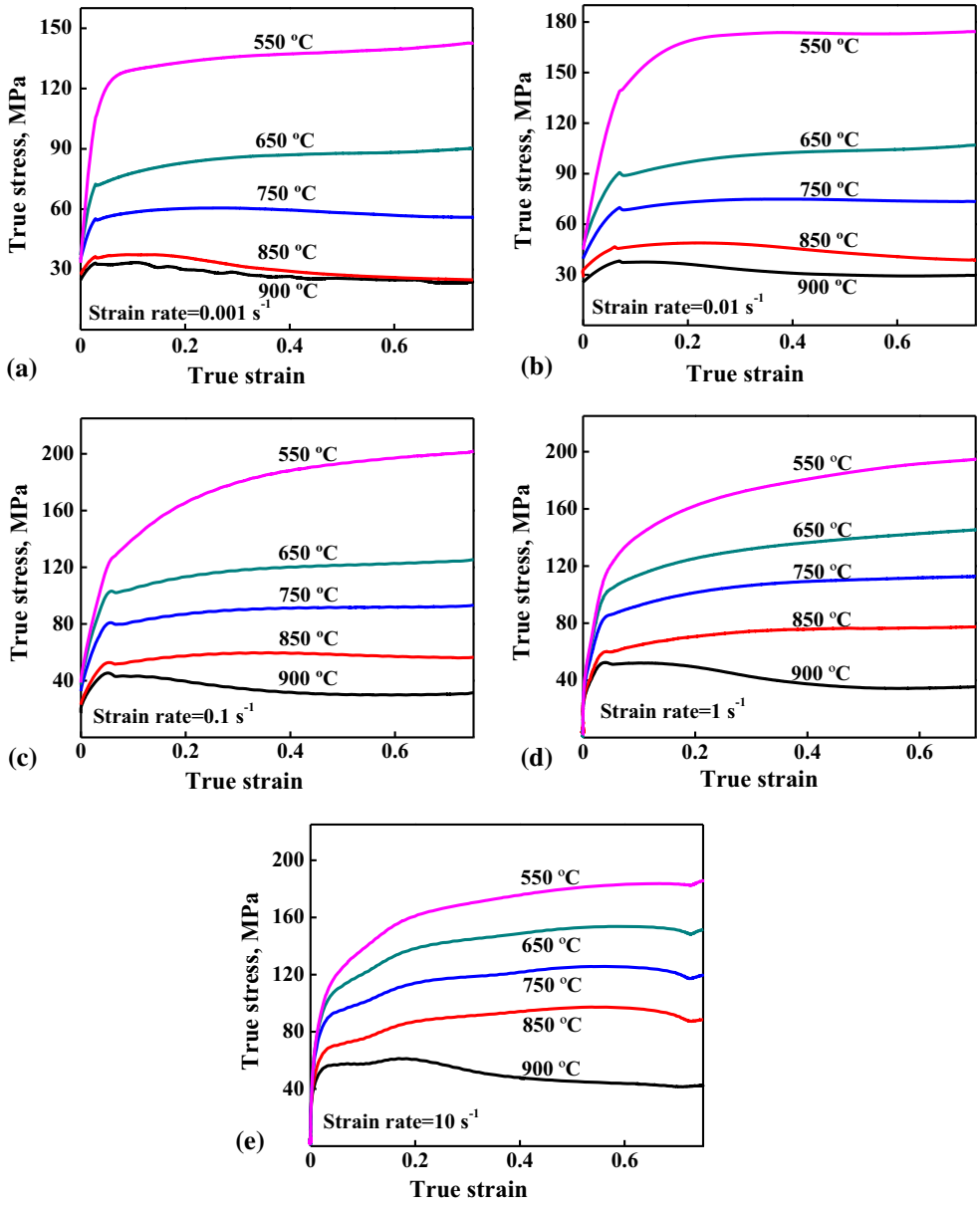

Fig. 1 True stress–strain curves of the Cu-Zr-Ce alloy obtained under different strain rates: (a) 0.001 s^{-1}; (b) 0.01 s^{-1}; (c) 0.1 s^{-1}; (d) 1 s^{-1} and (e) 10 s^{-1}

Calculating natural logarithms of the two sides of Eq 3 yields:

$$\ln[\sinh(\alpha\sigma)] = \frac{1}{n}\ln\dot{\varepsilon} + \frac{Q}{nR}\left(\frac{1}{T}\right) - \frac{1}{n}\ln A. \quad \text{(Eq 7)}$$

If $\dot{\varepsilon}$ is a constant, Eq 7 can be expressed as:

$$Q = R\left[\frac{\partial(\ln\dot{\varepsilon})}{\partial\ln[\sinh(\alpha\sigma)]}\right]_T\left[\frac{\partial\ln[\sinh(\alpha\sigma)]}{\partial(1/T)}\right]_{\dot{\varepsilon}} = RnS. \quad \text{(Eq 8)}$$

By plotting $\ln\dot{\varepsilon} - \ln[\sinh(\alpha\sigma)]$ and $\ln[\sinh(\alpha\sigma)] - 1/T$ at different temperatures, as shown in Fig. 2(c) and (d), and by calculating the slope of the linear regression lines value, the value of n is 14.499 and S is 4.551, respectively. Thus, the value of $Q = RnS = 548.658$ kJ/mol.

Almost no research results were found on hot compressive deformation behavior of the Cu-0.2%Zr alloy. However, many researchers investigated the Cu-Cr-Zr alloy and calculated the value of thermal activation energy Q for the Cu-0.4%Cr-0.1%Zr alloy (Ref 24), Cu-0.6%Cr-0.03%Zr alloy (Ref 25), Cu-0.4%Cr-0.15%Zr-0.05%Ce alloy (Ref 26) and Cu-0.36%Cr-0.03%Zr alloy (Ref 27) as 392.5, 572, 495.8 and 432.6 kJ/mol, respectively. The Q value of the Cu-0.2%Zr-0.15%Ce alloy is larger than the alloys without Ce. The addition of Ce may be the main reason for increasing Q. The addition of Ce can fix dislocations at the grain boundaries, and high dislocation density was obtained, a direct result of the deformation activation energy with more difficult dynamic recovery.

Calculating natural logarithms of the two sides of Eq 4 yields:

$$\ln Z = \ln A + n2\ln[\sinh(\alpha\sigma)]. \quad \text{(Eq 9)}$$

The relationship between $\ln Z$ and $\ln[\sinh(\alpha\sigma)]$ for the Cu-0.2%Zr-0.15%Ce alloy is shown in Fig. 2(e). The value of n_2

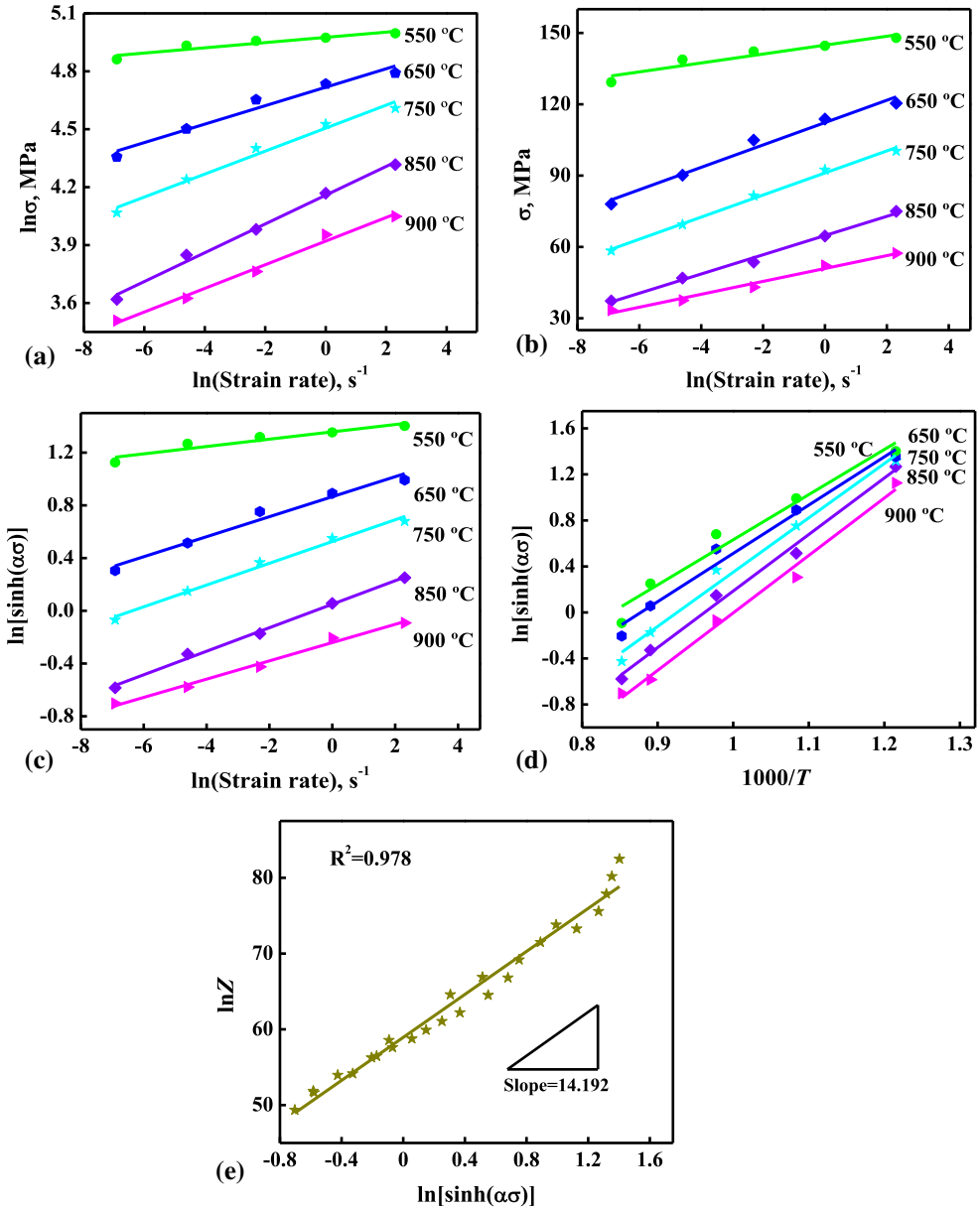

Fig. 2 Relationships between (a) lnσ and lnε; (b) σ and lnε; (c) lnε and ln[sinh($\alpha\sigma$)]; (d) 1/T and ln[sinh($\alpha\sigma$)]; (e) ln[sinh($\alpha\sigma$)] and ln$Z$

and its intercept represent the value of ln$A$ and can be evaluated by the slope of the straight line. Thus, the values of n_2 and A are 14.193 and 3.934×10^{25}, respectively.

According to the above analysis results, the deduced constitutive equation for the Cu-0.2%Zr-0.15%Ce alloy can be expressed as:

$$\dot{\varepsilon} = 3.934 \times 10^{25}[\sinh(0.0143\sigma)]^{14.193} \exp(-548.658/RT). \quad \text{(Eq 10)}$$

3.3 Compensation for Strain

Many researchers considered that the effects of strain on flow stress during high-temperature deformation were not important and usually ignored (Ref 28). However, many recent reports have indicated that the strain can strongly affect the material constants α, n, Q and A (Ref 29, 30). During the established constitutive model, the compensation for strain would be taken into consideration to improve the accuracy of the flow stress prediction. In this paper, variations of material constants with increasing strain were calculated. The values of the material constants were obtained at each strain in the 0.1-0.7 range with 0.05 interval. In order to visually represent the influence of strain on the materials constants, the obtained values were fitted by the fifth-order polynomials, as shown in Fig. 3. Then, the constitutive model of the alloy can be obtained as:

$$\begin{aligned} \alpha &= \alpha_0 + \alpha_1\varepsilon + \alpha_2\varepsilon^2 + \alpha_3\varepsilon^3 + \alpha_4\varepsilon^4 + \alpha_5\varepsilon^5, \\ n &= n_0 + n_1\varepsilon + n_2\varepsilon^2 + n_3\varepsilon^3 + n_4\varepsilon^4 + n_5\varepsilon^5, \\ Q &= Q_0 + Q_1\varepsilon + Q_2\varepsilon^2 + Q_3\varepsilon^3 + Q_4\varepsilon^4 + Q_5\varepsilon^5, \\ \ln A &= A_0 + A_1\varepsilon + A_2\varepsilon^2 + A_3\varepsilon^3 + A_4\varepsilon^4 + A_5\varepsilon^5. \end{aligned} \quad \text{(Eq 11)}$$

The fifth-order polynomial fitting results are given in Table 1. Once the materials constants are determined, the flow stress

will be predicted at a certain strain. Based on Eq 4, the constitutive equation including the flow stress and the Zener–Holloman parameter for the Cu-0.2%Zr-0.15%Ce alloy can be expressed as:

$$\begin{cases} \sigma = \frac{1}{\alpha}\ln\left\{\left(\frac{Z}{A}\right)^{1/n}+\left[\left(\frac{Z}{A}\right)^{2/n}+1\right]^{1/2}\right\} \\ Z = \dot{\varepsilon}\exp\left(\frac{Q}{RT}\right) \end{cases}. \quad \text{(Eq 12)}$$

3.4 Constitutive Equation Verification

According to the determined materials constants in Eq 11, predicted stress was obtained for all experimental conditions. The comparisons between the predicted value and experimental stress value at a given strain rate are shown in Fig. 4(a-e). The calculated results are consistent with the experimental results, indicating that the established constitutive model for the Cu-Zr-Ce alloy is predicting the flow stress fairly accurately.

Statistical parameters, such as correlation coefficient (R), mean squared error ($RMSE$) and average relative error ($AARE$), were used to evaluate the credibility of the established constitutive model. These are expressed as:

$$R = \frac{\sum_{i=1}^{N}(\sigma_e^i-\bar{\sigma}_e)(\sigma_p^i-\bar{\sigma}_p)}{\sqrt{\sum_{i=1}^{N}(\sigma_e^i-\bar{\sigma}_e)^2}\sqrt{\sum_{i=1}^{N}(\sigma_p^i-\bar{\sigma}_p)^2}}, \quad \text{(Eq 13)}$$

$$\mathrm{RMSE} = \sqrt{\frac{1}{N}\sum_{i=1}^{N}(\sigma_e^i-\sigma_P^i)^2}, \quad \text{(Eq 14)}$$

$$\mathrm{AARE}\,(\%) = \frac{1}{N}\sum_{i=1}^{N}\left|\frac{\sigma_e^i-\sigma_P^i}{\sigma_e^i}\right|\times 100. \quad \text{(Eq 15)}$$

Here, σ_e is the experimental flow stress, σ_p—predicted flow stress, $\bar{\sigma}_e$ and $\bar{\sigma}_p$—mean values of σ_e and σ_p, respectively. N is the total number of experimental data points. The correlation coefficient R is used to reflect the strength of the linear relationship between the predicted and experimental values. $RMSE$ is the standard error, and $AARE$ can be considered an unbiased statistic for evaluating the performance of the developed model. The relationship between the experimental and predicted flow stress results is shown in Fig. 4(f). Corresponding statistic values of R, $RMSE$ and $AARE$ were calculated to be 0.982, 4.142 and 4.87%, respectively. Very low values of $AARE$ and $RMSE$ indicate that the established constitutive model could give better prediction of the flow stress for the Cu-0.2%Zr-0.15%Ce alloy and can be used for the study of the hot compressive deformation process of the alloy.

3.5 Critical Strain for the Dynamic Recrystallization

At present, the initiation of DRX, called the critical strain, is before the peak strain in the stress–strain curve, which is accepted by many researchers (Ref 31). The critical strain for the initiation of DRX is important to describe DRX kinetics (Ref 32). Some researchers obtained the critical strain for DRX by observing the microstructure. While this method is accurate, it needs a heavy workload (Ref 33). Many researches (Ref 21, 34) show that using work hardening rate to confirm the critical strain of the onset for DRX is another available method, which

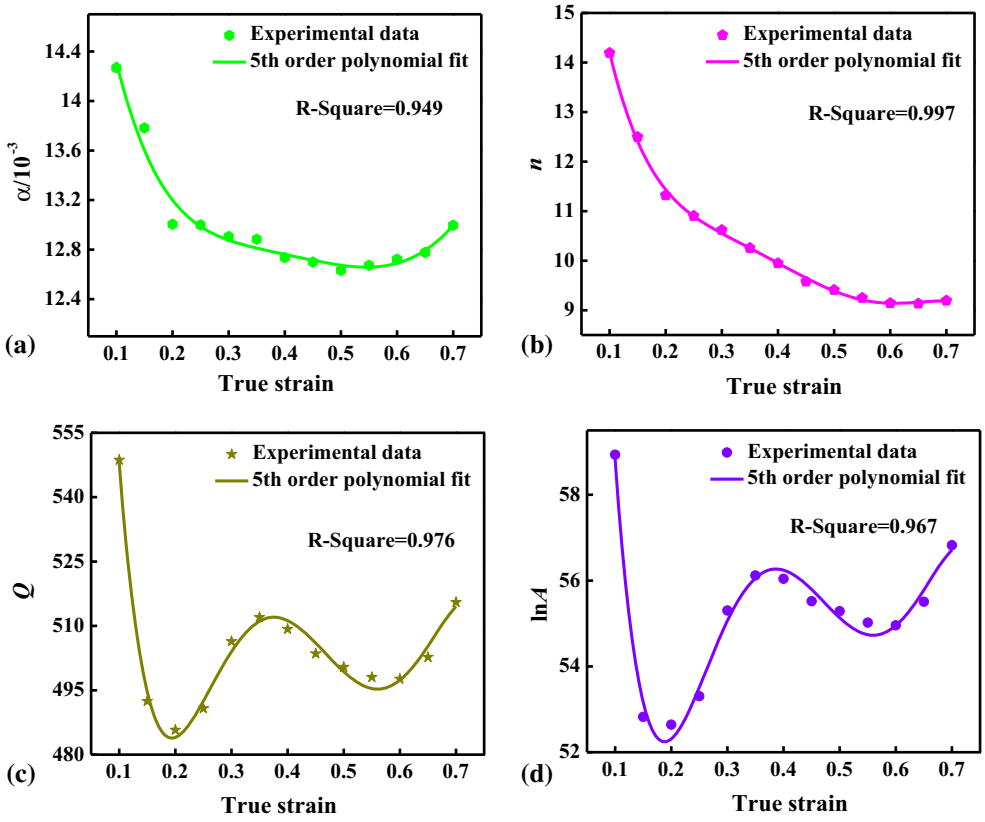

Fig. 3 Variation of: (a) α; (b) n; (c) Q, and (d) ln$A$ with true strain

Table 1 Fifth-order polynomial fitting results

ln*A*	*n*	*Q*	α
$A_0 = 101.7167$	$n_0 = 22.6847$	$Q_0 = 938.3684$	$\alpha_0 = 0.01736$
$A_1 = -754.2098$	$n_1 = -133.0068$	$Q_1 = -6820.3761$	$\alpha_1 = -0.04554$
$A_2 = 4177.2592$	$n_2 = 609.8537$	$Q_2 = 37441.1612$	$\alpha_2 = 0.1845$
$A_3 = -10385.0919$	$n_3 = -1423.9441$	$Q_3 = -93006.7083$	$\alpha_3 = -0.3696$
$A_4 = 11917.5227$	$n_4 = -1606.3663$	$Q_4 = 106814.9374$	$\alpha_4 = 0.3516$
$A_5 = -5136.0980$	$n_5 = -693.1665$	$Q_5 = -46056.5171$	$\alpha_5 = -0.0113$

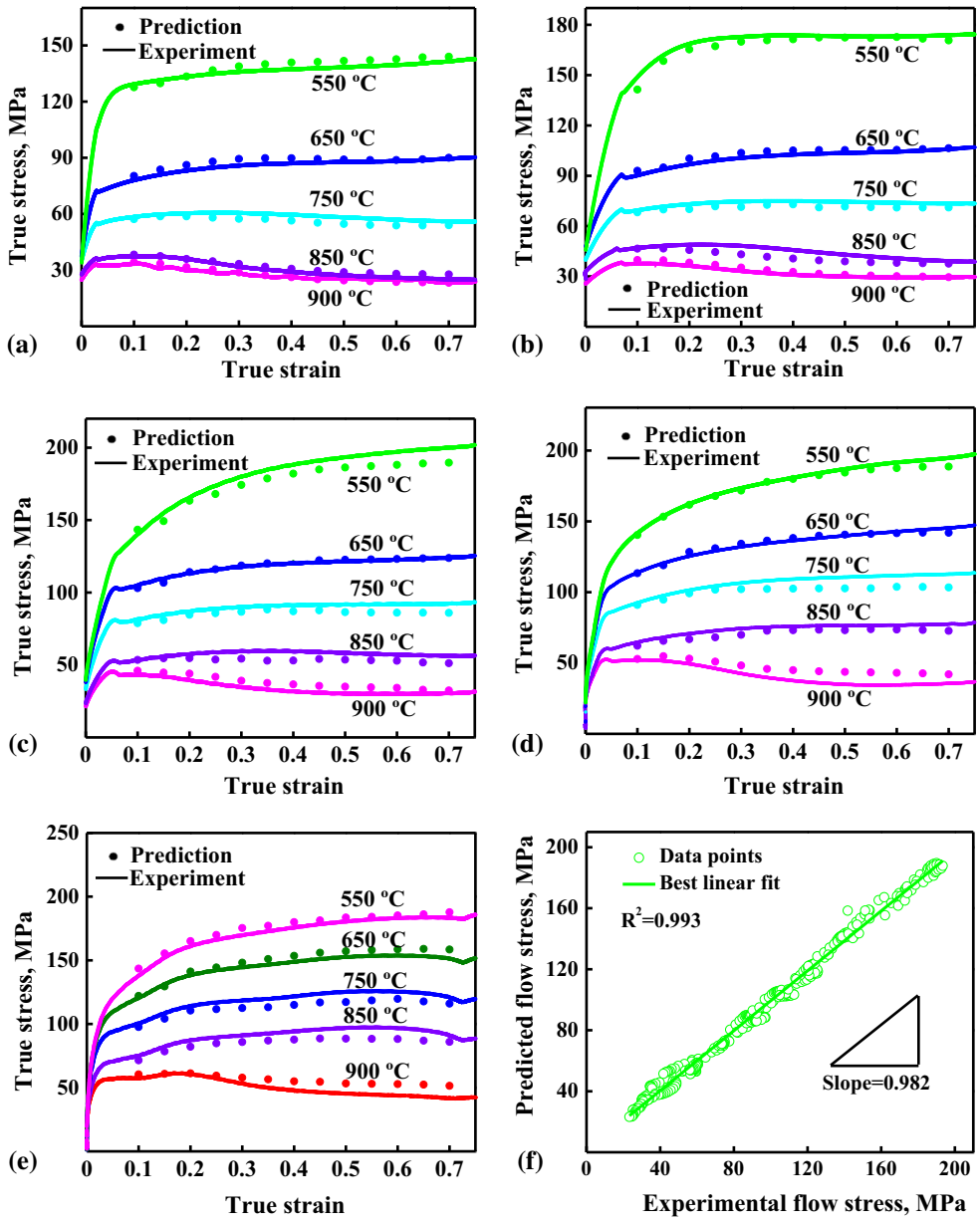

Fig. 4 Comparison between the predicted and experimental flow stress at the strain rate of: (a) 0.001 s^{-1}; (b) 0.01 s^{-1}; (c) 0.1 s^{-1}; (d) 1 s^{-1}; (e) 10 s^{-1} and (f) correlation between predicted and experimental flow stress values

has been more widely adopted. In this method, the inflection point of the $\ln\theta$-ε curve determines the critical strain for the onset of DRX, where θ is the work hardening rate (Ref 35). The $\ln\theta$-ε curves for the Cu-0.2%Zr-0.15%Ce alloy compressed at the strain rates of 0.001 and 10 s^{-1} under different temperatures are shown in Fig. 5(a) and (b), respectively. Zhang et al. (Ref 26) researched the Cu-Cr-Zr-Y alloy and drew similar curves using the same method. The third-order polynomials of the $\ln\theta$-ε curve ($-\partial(\ln\theta)/\partial\varepsilon - \varepsilon$ versus ε curve) are shown in Fig. 5(c) and (d). The inflection points of the $\ln\theta$-ε curves and $-\partial(\ln\theta)/\partial\varepsilon - \varepsilon$ versus ε curve are marked by arrows. From the two figures, the critical strain for the onset of DRX

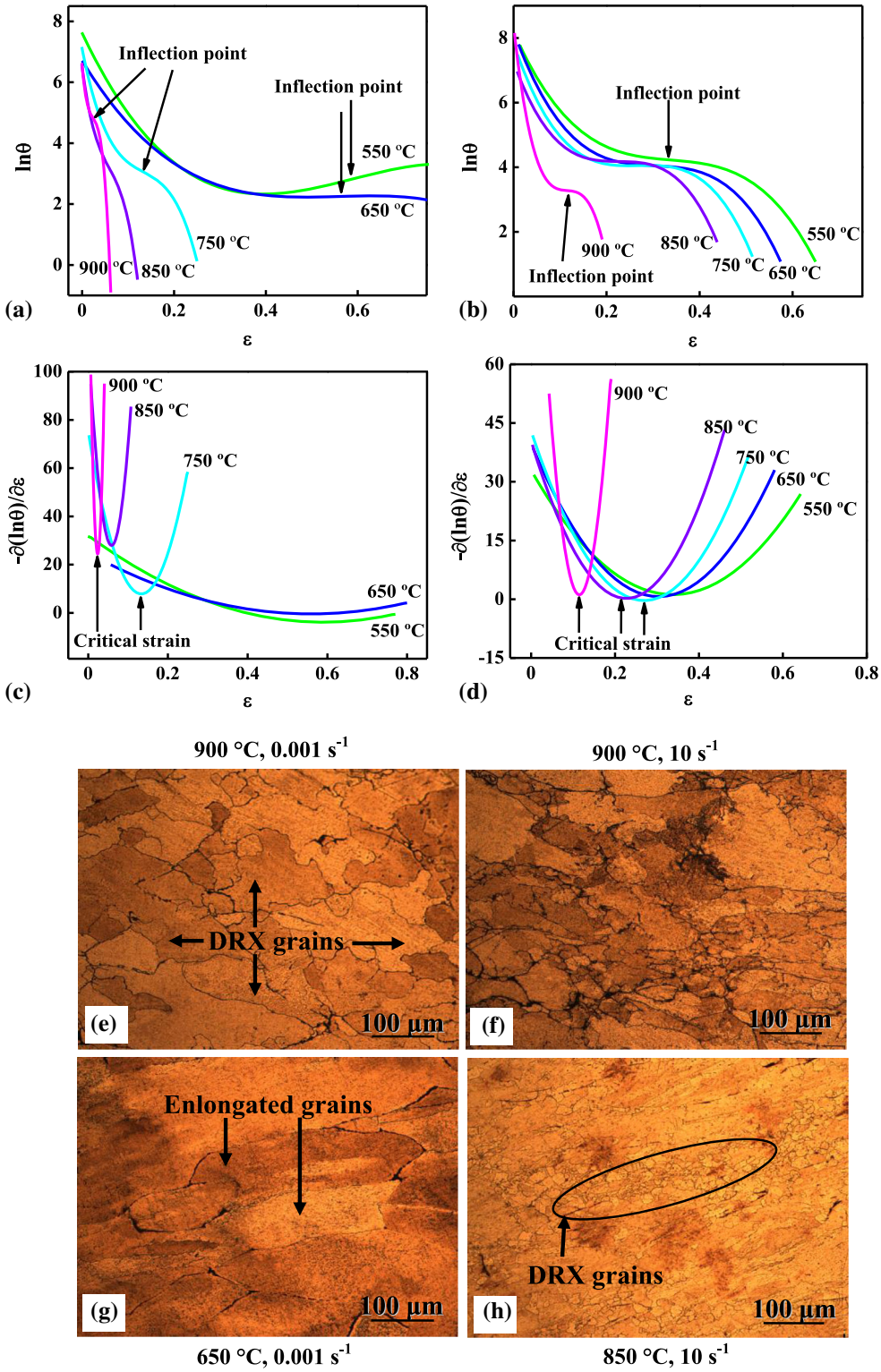

Fig. 5 Relationships between $\ln\theta$ and ε; $-\partial(\ln\theta)/\partial\varepsilon$ and ε at: (a, c) 0.001 s^{-1}; (b, d) 10 s^{-1} and microstructure under different critical strain: (e) 900 °C, 0.001 s^{-1}; (f) 900 °C, 10 s^{-1}; (g) 650 °C, 0.001 s^{-1}; (h) 850 °C, 0.001 s^{-1}

increases with the temperature drop. This indicates that higher temperature promotes DRX because the nucleation ratio of recrystallization and the growth rate increase. Sun et al. (Ref 32) came up with the same conclusion in the research of DRX of the Cu-Ni-Si-Ag alloy by the work hardening rate method. In Fig. 5, the minimum point stands for the critical strain (ε_c) for DRX onset. Optical microstructure obtained under different critical strain is shown in Fig. 5(e-h). At low temperature of 650 °C, elongated grains were observed. With the temperature increase, some DRX grains were found at the grain boundaries

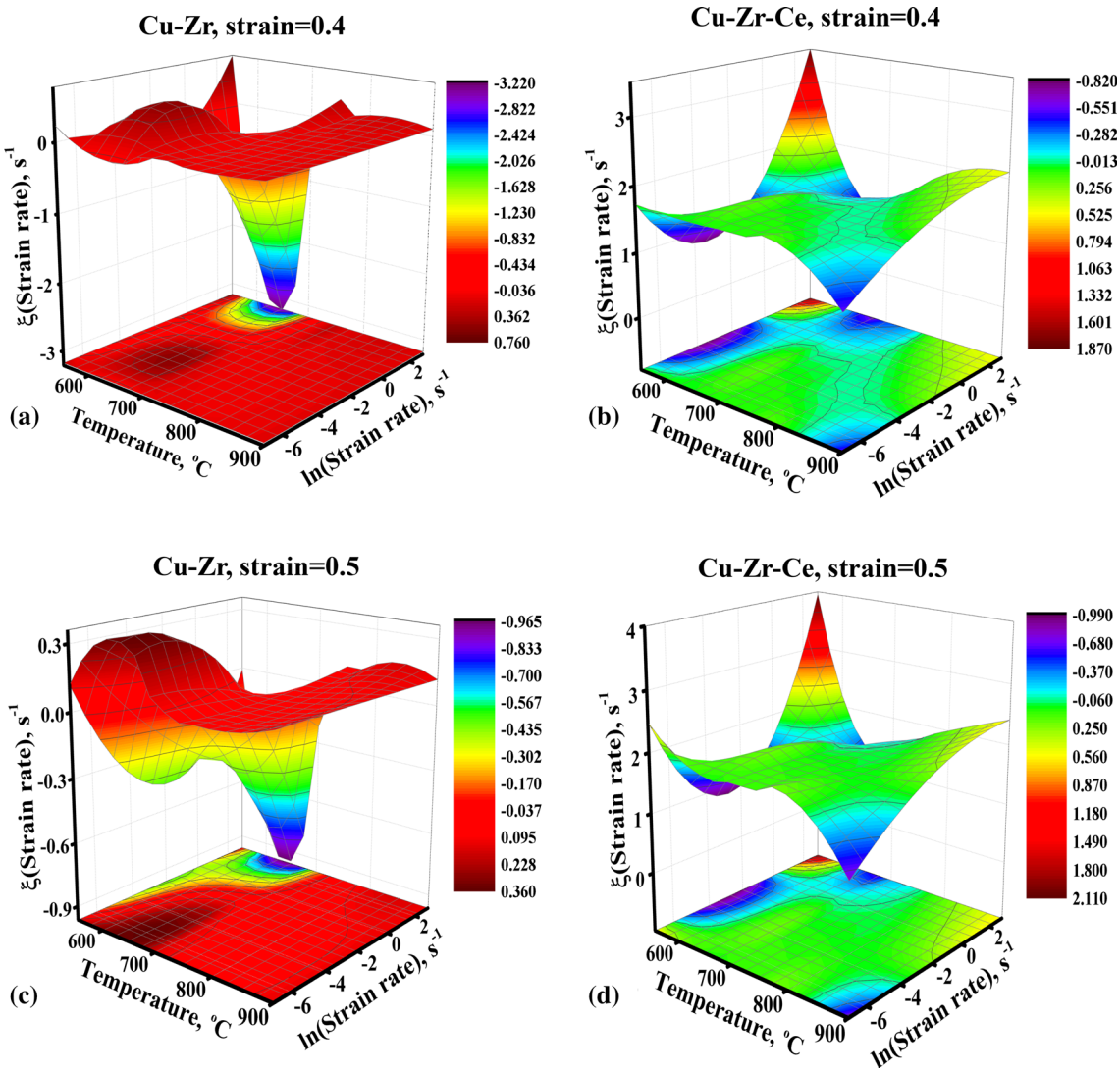

Fig. 6 3D surfaces of the $\xi(\dot{\varepsilon})$ value for Cu-Zr and Cu-Zr-Ce alloys versus the strain rate and temperature at true strains of: (a-b) 0.4 and (c-d) 0.5

in Fig. 5(h), marked by an arrow. At high temperature of 900 °C, the uniform grains can be clearly observed. Comparing Fig. 5(e) and (f), the DRX behavior is more pronounced at lower strain rate. The critical strain-related microstructure means that the accumulated energy for nucleation and DRX grains growth at lower temperature and higher strain rate is insufficient.

4. Discussion

4.1 Ce Addition Effects on Processing Maps

Processing maps are plotted based on the DMM, an analysis method, which regards the studied material as a nonlinear power system (Ref 36). According to Prasad, the energy input in the system during hot deformation was dissipated and the total power (P) can fall into dissipative quantity (G) and dissipation by association (J), defined as:

$$P = J + G = \sigma\dot{\varepsilon} = \int_0^{\sigma} \dot{\varepsilon}\mathrm{d}\sigma + \int_0^{\dot{\varepsilon}} \sigma\mathrm{d}\dot{\varepsilon}. \quad \text{(Eq 16)}$$

In this model, J and G can be confirmed with the strain rate sensitivity parameter m, which can be expressed as (Ref 37):

$$\left(\frac{\partial J}{\partial G}\right)_{\dot{\varepsilon},T} = \frac{\partial P}{\partial G}\frac{\partial J}{\partial P} = \frac{\sigma\mathrm{d}\dot{\varepsilon}}{\dot{\varepsilon}\mathrm{d}\sigma} = \left[\frac{\partial(\ln\sigma)}{\partial(\ln\dot{\varepsilon})}\right]_{\dot{\varepsilon},T} = m. \quad \text{(Eq 17)}$$

For the ideal linear dissipation process, $m = 1$ and $J = J_{\max} = \sigma\dot{\varepsilon}/2 = P/2$, and the efficiency of energy dissipation (η) is defined as (Ref 38):

$$\eta = \frac{J}{J_{\max}} = \frac{2m}{m+1}. \quad \text{(Eq 18)}$$

Applying the irreversible maximum principle to the severe plastic deformation, the flow instability criteria based on DMM can be defined as follows (Ref 39):

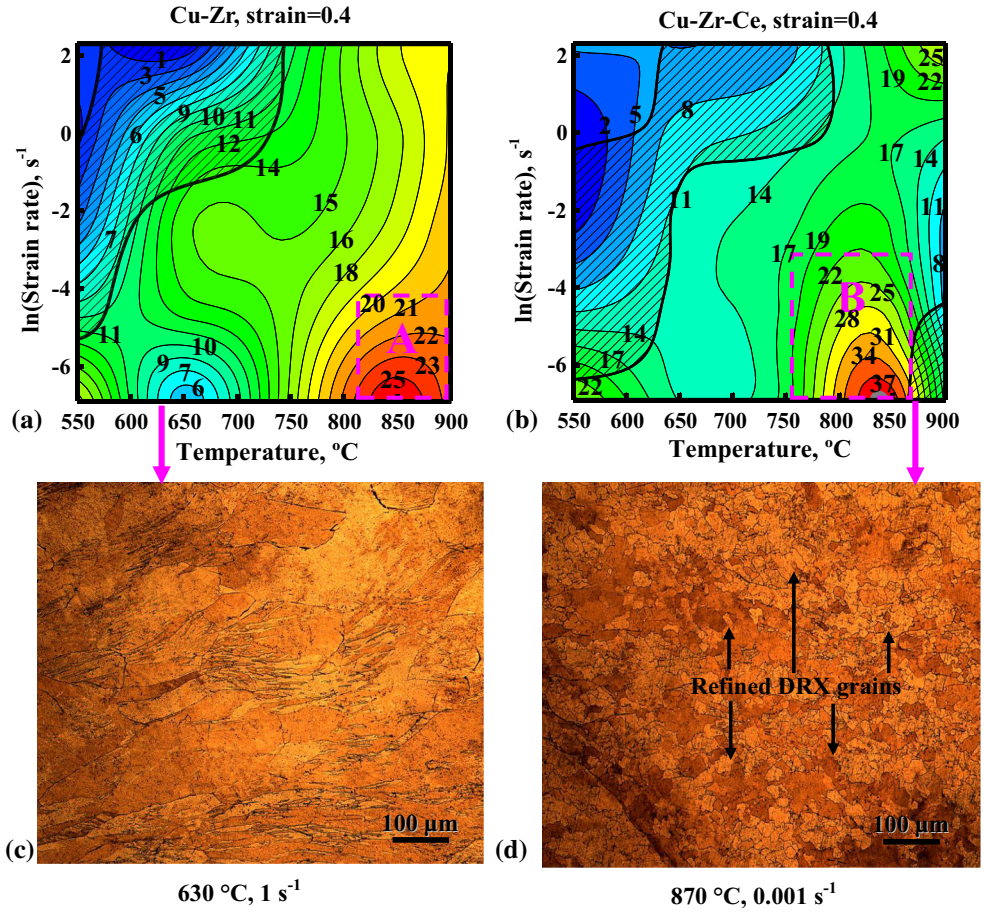

Fig. 7 Processing maps of: (a) the Cu-Zr alloy and (b) the Cu-Zr-Ce alloy at true strain of 0.4, and (c-d) microstructure at corresponding deformation conditions

$$\xi(\dot{\varepsilon}) = \frac{\partial \ln\left(\frac{m}{m+1}\right)}{\partial \ln \dot{\varepsilon}} + m < 0. \quad \text{(Eq 19)}$$

The variation of the instability parameter $\xi(\dot{\varepsilon})$ with the test temperature and strain rate can be presented with the instability map. Figure 6 shows 3D instability parameter $\xi(\dot{\varepsilon})$ map for the Cu-0.2%Zr-0.15%Ce alloy. The flow instability occurs when the value of $\xi(\dot{\varepsilon})$ becomes negative. It can be seen that the instability parameter $\xi(\dot{\varepsilon})$ decreased, while the strain increased from Fig. 6(a) and (c) or Fig. 6(b) and (d). Comparing Fig. 6(a) and (b), negative values of the instability parameter $\xi(\dot{\varepsilon})$ for the Cu-0.2%Zr-0.15%Ce alloy are less than for the Cu-0.2%Zr alloy. The same result can be obtained from Fig. 6(c) and (d). This means that the hot workability of the Cu-0.2%Zr alloy has been optimized by the addition of Ce.

The processing maps for the Cu-0.2%Zr and Cu-0.2%Zr-0.15%Ce alloys deformed at the strain of 0.4 are shown in Fig. 7(a) and (b), respectively. A stable domain in the 800-900 °C temperature and 0.001-0.01 s^{-1} strain rate ranges can be found in the processing map of the Cu-0.2%Zr alloy, with a peak efficiency of about 25% at about 850 °C and 0.001 s^{-1} in the domain A marked by the red rectangle in Fig. 7(a). A similar stable domain B marked by the red rectangle was observed for the Cu-Zr-Ce alloy in Fig. 7(b), and it is in the 750-870 °C deformation temperature range and 0.001-0.1 s^{-1} strain rate range, with the peak efficiency of about 37% at about 850 °C and 0.001 s^{-1}. Comparing the domains A and B, the dissipation factor increased by 32.4% because the Ce addition can effectively promote microstructure evolution. Much higher peak efficiency represents the excellent hot workability of the Cu-0.2%Zr-0.155Ce alloy. It also represents that the addition of Ce can optimize the performance of hot workability of the Cu-0.2%Zr alloy. The unstable domains are demonstrated with the shaded regions and contour lines in the hot processing map represent the efficiency of energy dissipation in Fig. 7. Similar unstable regions were observed at low deformation temperatures and high strain rates for the two alloys. Many research results report that the instability microstructure can be found in the unstable regions (Ref 37). Thus, the conditions for hot processing, which are located in flow instability regions, should be avoided.

4.2 Effects of Ce Addition on Microstructure Evolution

The evolution of microstructure for the two alloys is presented in Fig. 7(c) and (d). In Fig. 7(c), the original elongated grains were found and the recrystallized grains cannot be observed when the Cu-0.2%Zr alloy was deformed at 640 °C and 1 s^{-1} strain rate. However, many smaller DRX structures appear when the Cu-0.2%Zr-0.15%Ce alloy was compressed at 870 °C and 0.001 s^{-1} strain rate, as shown in Fig. 7(d). This also indicates that the addition of Ce can effectively refine the grains and promote DRX.

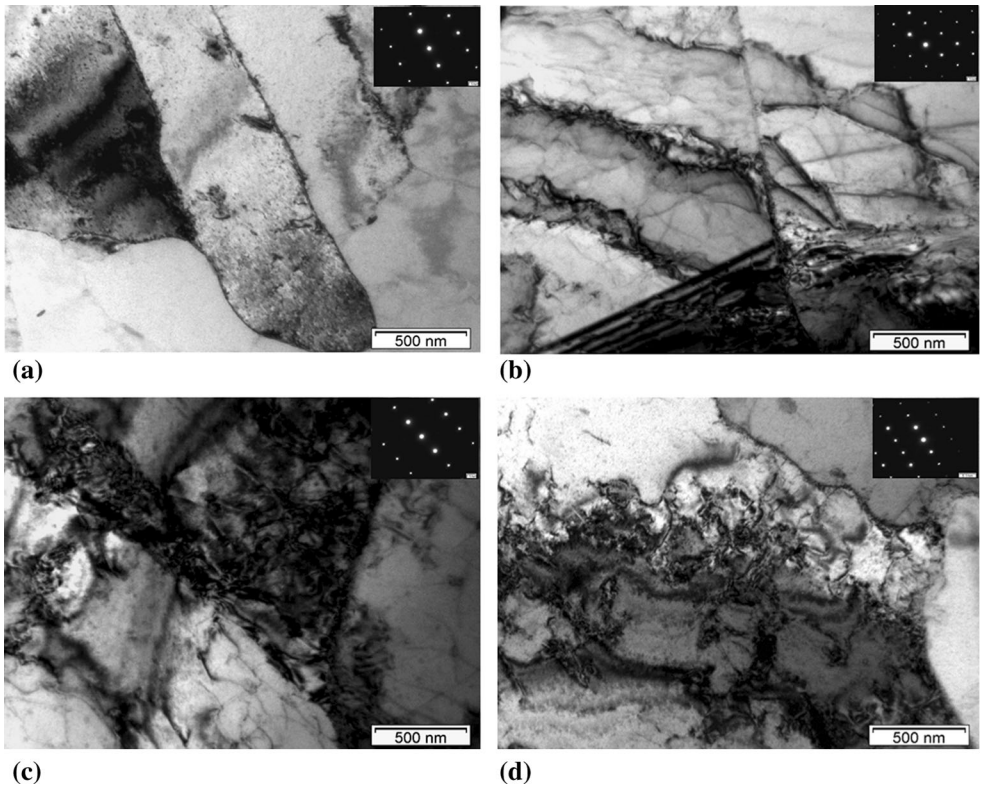

Fig. 8 TEM micrographs of: (a, c) Cu-Zr and (b, d) Cu-Zr-Ce alloys deformed at different conditions: (a) 650 °C and 0.1 s^{-1}; (b) 650 °C and 0.1 s^{-1}; (c) 850 °C and 0.001 s^{-1}; (d) 850 °C and 0.001 s^{-1}

Figure 8 shows transmission electron micrographs (TEM) of the Cu-0.2%Zr and Cu-0.2%Zr-0.15%Ce alloys compressed at different conditions. Comparing the diffraction patterns in Fig. 8, a larger interplanar spacing can be found in the Cu-0.2%Zr alloy, which means that the dislocation density of the Cu-0.2%Zr-0.15%Ce alloy is much higher than that of the Cu-Zr alloy (Ref 40). Thus, it can be concluded that the addition of Ce can accelerate the formation of dislocations at the same compressive conditions in Fig. 8(a) and (b). The same phenomenon is observed in Fig. 8(c) and (d). With increasing dislocation density, the accumulated energy increased with the Ce addition. Thus, the existence of accumulated energy and dislocations can improve the driving force of recrystallized nucleation. This means that the addition of Ce is beneficial for the hot working of the Cu-Zr alloy.

5. Conclusions

Hot compressive behavior of Cu-0.2%Zr-0.15%Ce alloy was studied using hot compression tests over a wide range of compressive strain rates and temperatures. The following conclusions can be drawn:

1. The flow stress of Cu-0.2%Zr-0.15%Ce alloy is sensitive to strain rate and temperature. The flow stress increases with decreasing deformation temperature and increasing strain rate.
2. The effect of the strain on material constants α, n, Q and ln A was considered, and constitutive equation for the Cu-0.2%Zr-0.15%Ce alloy has been developed according to the Arrhenius equation. The effect of the strain on material constants was expressed with the fifth-order polynomial equations with good fitting correlation.
3. The performance of developed constitutive model for the Cu-0.2%Zr-0.15%Ce alloy was evaluated by the average absolute relative error (*AARE*), the root-mean-square error (*RMSE*) and the correlation coefficient (*R*). The values of *R*, *RMSE* and *AARE* were 0.982, 4.142 and 4.87%, respectively, indicating that the developed constitutive model has good prediction capability.
4. The critical strain conditions for DRX were confirmed using the method of strain hardening rate. Microstructure was observed under critical conditions. Deformation strain rate and temperature can strongly affect deformed microstructure. The processing maps of the Cu-0.2%Zr and Cu-0.2%Zr-0.15%Ce alloys at the strain of 0.4 and 0.5 were established. Optimal processing parameters for the two alloys are in the 800-900 °C temperature range and 0.001-0.01 s^{-1} strain rate range for the Cu-0.2%Zr alloy, and in the 750-870 °C temperature range and 0.001-0.1 s^{-1} strain rate range for the Cu-0.2%Zr-0.15%Ce alloy. The addition of Ce can optimize the hot workability of the Cu-0.2%Zr alloy.

Acknowledgments

This work was supported by the National Natural Science Foundation of China (51101052) and the National Science Foundation (IRES 1358088).

References

1. J.R. Davis, *Copper and Copper Alloys. ASM Specialty Handbook* (ASM International, USA, 2001), p. 153
2. L.M. Bi, P. Liu, X.H. Chen, X.K. Liu, W. Li, and F.C. Ma, Analysis of Phase in Cu-15%Cr-0.24%Zr Alloy, *Trans. Nonferrous Met. Soc. China*, 2013, **23**(5), p 1342
3. Y. Zhang, A.A. Volinsky, H.T. Tran, Z. Chai, P. Liu, B.H. Tian, and Y. Liu, Aging Behavior and Precipitates Analysis of the Cu-Cr-Zr-Ce Alloy, *Mater. Sci. Eng. A*, 2016, **650**, p 248
4. J.H. Su, Q.M. Dong, P. Liu, H.J. Li, and B.X. Kang, Research on Aging Precipitation in a Cu-Cr-Zr-Mg Alloy, *Mater. Sci. Eng. A*, 2005, **392**(1), p 422
5. L.K.L. Falk, P.R. Howell, G.L. Dunlop, and T.G. Langdon, The Role of Matrix Dislocations in the Superplastic Deformation of a Copper Alloy, *Acta Metall.*, 1986, **34**(7), p 1203
6. S.C. Krishna, G.S. Rao, A.K. Jha, B. Pant, and P.V. Venkitakrishnan, Strengthening in High Strength Cu-Cr-Zr-Ti Alloy Plates Produced by Hot Rolling, *Mater. Sci. Eng. A*, 2016, **674**, p 164
7. A.Y. Khereddine, F.H. Larbi, H. Azzeddine, T. Baudin, F. Brisset, A.L. Helbert, M.H. Mathon, M. Kawasaki, D. Bradai, and T.G. Langdon, Microstructures and Textures of a Cu-Ni-Si Alloy Processed by High-Pressure Torsion, *J. Alloys Compd.*, 2013, **574**, p 361
8. H. Zhang, H.G. Zhang, and L.X. Li, Hot Deformation Behavior of Cu-Fe-P Alloys During Compression at Elevated Temperatures, *J. Mater. Process. Technol.*, 2009, **209**(6), p 2892
9. L.J. Peng, H.F. Xie, G.J. Huang, Y.F. Li, X.Q. Yin, X. Feng, X.J. Mi, and Z. Yang, The Phase Transformation and Its Effects on Properties of a Cu-0.12 wt.%Zr Alloy, *Mater. Sci. Eng. A*, 2015, **633**, p 28
10. Y. Ye, X. Yang, J. Wang, X. Zhang, Z. Zhang, and T. Sakai, Enhanced Strength and Electrical Conductivity of Cu-Zr-B Alloy by Double Deformation-Aging Process, *J. Alloys Compd.*, 2014, **615**, p 249
11. J. Wongsa-Ngam, M. Kawasaki, Y. Zhao, and T.G. Langdon, Microstructural Evolution and Mechanical Properties of a Cu-Zr Alloy Processed by High-Pressure Torsion, *Mater. Sci. Eng. A*, 2011, **528**(25-6), p 7715
12. V.A. Phillips, Electron Microscope Observations on Precipitation in a Cu-1.07 %Zr Alloy, *Metallography*, 1974, **7**(2), p 137
13. K. Wang, K.F. Liu, and J.B. Zhang, Microstructure and Properties of Aging Cu-Cr-Zr Alloy, *Rare Met.*, 2014, **33**(2), p 134
14. Z. Yang, F. Zhang, C. Zheng, M. Zhang, B. Lv, and L. Qu, Study on Hot Deformation Behaviour and Processing Maps of Low Carbon Bainitic Steel, *Mater. Des.*, 2015, **66**, p 258
15. B. Li, Q. Pan, and Z. Yin, Microstructural Evolution and Constitutive Relationship of Al-Zn-Mg Alloy Containing Small Amount of Sc and Zr During Hot Deformation Based on Arrhenius-Type and Artificial Neural Network Models, *J. Alloys Compd.*, 2014, **584**, p 406
16. Y. Lin and X.M. Chen, A Critical Review of Experimental Results and Constitutive Descriptions for Metals and Alloys in Hot Working, *Mater. Des.*, 2011, **32**(4), p 1733
17. Y. Zhang, B.H. Tian, A.A. Volinsky, H.L. Sun, Z. Chai, P. Liu, X.H. Chen, and Y. Liu, Dynamic Recrystallization Model of the Cu-Cr-Zr-Ag Alloy Under Hot Deformation, *J. Mater. Res.*, 2016, **31**, p 1275
18. C.M. Sellars and W.J. Mctegart, On the Mechanism of Hot Deformation, *Acta Metall.*, 1966, **14**(9), p 1136
19. N. Haghdadi, A. Zarei-Hanzaki, and H.R. Abedi, The Flow Behavior Modeling of Cast A356 Aluminum Alloy at Elevated Temperatures Considering the Effect of Strain, *Mater. Sci. Eng. A*, 2012, **535**, p 252
20. Y. Cao, H. Di, R.D.K. Misra, X. Yi, J.C. Zhang, and T.J. Ma, On the Hot Deformation Behavior of AISI, 420 Stainless Steel Based on Constitutive Analysis and CSL Model, *Mater. Sci. Eng. A*, 2014, **593**, p 111
21. Y. Zhang, H.L. Sun, A.A. Volinsky, B.H. Tian, Z. Chai, P. Liu, and Y. Liu, Hot Deformation and Dynamic Recrystallization Behavior of the Cu-Cr-Zr-Y Alloy, *J. Mater. Eng. Perform.*, 2016, **25**(3), p 1150
22. A. Galiyev, R. Kaibyshev, and G. Gottstein, Correlation of Plastic Deformation and Dynamic Recrystallization in Magnesium Alloy ZK60, *Acta Mater.*, 2001, **49**(7), p 1199
23. C. Zener and J.H. Hollomon, Effect of Strain Rate Upon Plastic Flow of Steel, *J. Appl. Phys.*, 1944, **15**(1), p 22
24. Y.H. Xiao, C. Guo, and X.Y. Guo, Constitutive Modeling of Hot Deformation Behavior of H62 Brass, *Mater. Sci. Eng. A*, 2011, **528**(21), p 6510
25. Z.Y. Ding, S.G. Jia, P.F. Zhao, M. Deng, and K.X. Song, Hot Deformation Behavior of Cu-0.6 Cr-0.03 Zr Alloy During Compression at Elevated Temperatures, *Mater. Sci. Eng. A*, 2013, **570**, p 87
26. Y. Zhang, A.A. Volinsky, H.T. Tran, Z. Chai, P. Liu, and B.H. Tian, Effects of Ce Addition on High Temperature Deformation Behavior of Cu-Cr-Zr Alloys, *J. Mater. Eng. Perform.*, 2015, **24**(10), p 3783
27. G.L. Ji, Q. Li, K.Y. Ding, L. Yang, and L. Li, A Physically-Based Constitutive Model for High Temperature Deformation of Cu-0.36 Cr-0.03 Zr Alloy, *J. Alloys Compd.*, 2015, **648**, p 397
28. C.L. Gan, Y.D. Xue, and M.J. Wang, Prediction of the Flow Stress of Al6061 at Hot Deformation Conditions, *Mater. Sci. Eng. A*, 2011, **528**, p 4199
29. Y.C. Lin, M.S. Chen, and J. Zhong, Constitutive Modeling for Elevated Temperature Flow Behavior of 42CrMo Steel, *Comp. Mater. Sci.*, 2008, **42**(3), p 470
30. Z.W. Cai, F.X. Chen, and J.Q. Guo, Constitutive Model for Elevated Temperature Flow Stress of AZ41M Magnesium Alloy Considering the Compensation of Strain, *J. Alloys Compd.*, 2015, **648**, p 215
31. E.I. Poliak and J.J. Jonas, Critical Strain for Dynamic Recrystallization in Variable Strain Rate Hot Deformation, *ISIJ Int.*, 2003, **43**, p 684
32. H.L. Sun, Y. Zhang, A.A. Volinsky, B.J. Wang, B.H. Tian, Z. Chai, and Y. Liu, Effects of Ag Addition on Hot Deformation Behavior of Cu-Ni-Si Alloys. *Adv. Eng. Mater.* 2017, **19**(3). https://doi.org/10.1002/adem.201600607
33. H. Mirzadeh and A. Najafizadeh, Prediction of the Critical Conditions for Initiation of Dynamic Recrystallization, *Mater. Des.*, 2010, **31**(3), p 1174
34. G.J. Huang, B.H. Qian, L.Y. Wang, and J.J. Jonas, Study on the Critical Conditions for Initial Dynamic Recrystallization of AZ31 Magnesium Alloy, *Rare Met. Mater. Eng.*, 2007, **36**(12), p 2080
35. E.S. Puchi-Cabrera, M.H. Staia, J.D. Guerin, J. Lesage, M. Dubar, and D. Chicot, Analysis of the Work-Hardening Behavior of C-Mn Steels Deformed Under Hot-Working Conditions, *Int. J. Plast*, 2013, **51**, p 145
36. Y.V.R.K. Prasad and T. Seshacharyulu, Processing Maps for Hot Working of Titanium Alloys, *Mater. Sci. Eng. A*, 1998, **243**, p 82
37. T.D. Kil, J.M. Lee, and Y.H. Moon, Quantitative Formability Estimation of Ring Rolling Process by Using Deformation Processing Map, *J. Mater. Process. Technol.*, 2015, **220**, p 224
38. T. Xi, C.G. Yang, M.B. Shahzad, and K. Yang, Study of the Processing Map and Hot Deformation Behavior of a Cu-Bearing 317LN Austenitic Stainless Steel, *Mater. Des.*, 2015, **87**, p 303
39. D.J. Li, Y.R. Feng, Z.F. Yin, F.S. Shangguan, K. Wang, Q. Liu, and F. Hu, Prediction of Hot Deformation Behaviour of Fe-25Mn-3Si-3Al TWIP Steel, *Mater. Sci. Eng. A*, 2011, **528**(28), p 8084
40. Y. Zhang, B.H. Tian, A.A. Volinsky, X.H. Chen, H.L. Sun, Z. Chai, P. Liu, and Y. Liu, Dynamic Recrystallization Model of the Cu-Cr-Zr-Ag Alloy Under Hot Deformation, *J. Mater. Res.*, 2016, **31**(9), p 1275